Check for updates

Effect of Re promoter on the structure and catalytic performance of Ni–Re/Al₂O₃ catalysts for the reductive amination of monoethanolamine†

Lei Ma,[abd] Li Yan,*[b] An-Hui Lu [ID] [a] and Yunjie Ding [ID] *[bc]

In this paper, Ni/Al₂O₃ catalysts (15 wt% Ni) with different Re loadings were prepared to investigate the effect of Re on the structure and catalytic performance of Ni–Re/Al₂O₃ catalysts for the reductive amination of monoethanolamine. Reaction results reveal that the conversion and ethylenediamine selectivity increase significantly with increasing Re loading up to 2 wt%. Ni–Re/Al₂O₃ catalysts show excellent stability during the reductive amination reaction. The characterization of XRD, DR UV-Vis spectroscopy, H₂-TPR, and acidity–basicity measurements indicates that addition of Re improves the Ni dispersion, proportion of octahedral Ni²⁺ species, reducibility, and acid strength for Ni–Re/Al₂O₃ catalysts. The Ni15 and Ni15–Re2 catalysts were chosen for in-depth study. The results from SEM-BSE, TEM, and CO-TPD indicate that smaller Ni⁰ particle size and higher Ni⁰ surface area are obtained in the reduced Ni–Re/Al₂O₃ catalysts. Results from *in situ* XPS and STEM-EDX line scan suggest that Re species show a mixture of various valances and have a tendency to aggregate on the surface of Ni⁰ particles. During reaction, the Ni⁰ particles on the Al₂O₃ support are stabilized and the sintering process is effectively suppressed by the incorporation of Re. It could be concluded that sufficient Ni⁰ sites, the collaborative effect of Ni–Re, and brilliant stability contribute to the excellent catalytic performance of Ni–Re/Al₂O₃ catalysts for the reductive amination of monoethanolamine.

Introduction

Ethylene amines is the collective name for ethylenediamine (EDA), polyethylene polyamines, and the cyclic amines, including piperazine (PIP), aminoethyl piperazine (AEP), and hydroxyethyl piperazine (HEP) *etc.* As an important intermediate, ethylene amines have wide applications in the production of pharmaceuticals, lube oil additives, chelating agents, fungicides, oil field chemicals, paper wet-strength resins, surfactants, and fabric softeners. Reductive amination of monoethanolamine (MEA) to ethylene amines is a common synthesis route which has been applied in industrial production process since the 1960s.[1–4] The reductive amination method has gained increasing interest since it constitutes a green economy route for the synthesis of ethylene amines.[5–14]

In the reductive amination process, ethylene amines are synthesized by contacting MEA and ammonia under hydrogen atmosphere in the presence of hydrogenation–dehydrogenation metal catalysts. The reaction pathways for the transformation of MEA to ethylene amines on a metal catalyst are postulated as follows: firstly, dehydrogenation of MEA to 2-amino-acetaldehyde; secondly, condensation with ammonia or an amine to form imine; lastly, hydrogenation of imine to amine.[7,8,11,15] The hydrogenation and dehydrogenation processes are catalyzed by the transition metal, while the condensation process could be accelerated by acid or base sites.[16–19] The presence of small amount of hydrogen is found to be necessary to maintain the activity of catalyst during the reductive amination process.[8,20,21] The dashed box in Fig. 1 indicates the main reaction path for the generation of EDA. Moreover, the product amines could continue to take part in the reductive amination process as reactants. The presence of continuous reaction makes the pathways more complicated and decreases the selectivity of the desired amine. As a result, the production of various by-products increases the cost of separation process. For this reason, it's important for the catalyst to have both high activity and selectivity of the desired product, such as EDA.

Different catalytic metal systems such as Ni,[17–19,21–24] Ni–Re,[25–29] Co,[20,30,31] Cu,[32–35] Fe,[36–38] Rh,[39,40] Ru,[12,13,41,42] Pt,[43–45] and Pd[46] *etc.* have been tested in the reductive amination of amino

[a]*State Key Laboratory of Fine Chemicals, School of Chemical Engineering, Dalian University of Technology, No. 2 Linggong Road, Dalian 116024, P. R. China*

[b]*Dalian National Laboratory for Clean Energy, Dalian Institute of Chemical Physics, Chinese Academy of Sciences, 457 Zhongshan Road, Dalian, 116023, China. E-mail: dyj@dicp.ac.cn; Fax: +86 411 84379143; Tel: +86 411 84379143*

[c]*State Key Laboratory of Catalysis, Dalian Institute of Chemical Physics, Chinese Academy of Sciences, 457 Zhongshan Road, Dalian, 116023, China*

[d]*University of Chinese Academy of Sciences, No. 19A Yuquan Road, Beijing 100049, China*

† Electronic supplementary information (ESI) available. See DOI: 10.1039/c7ra12891f
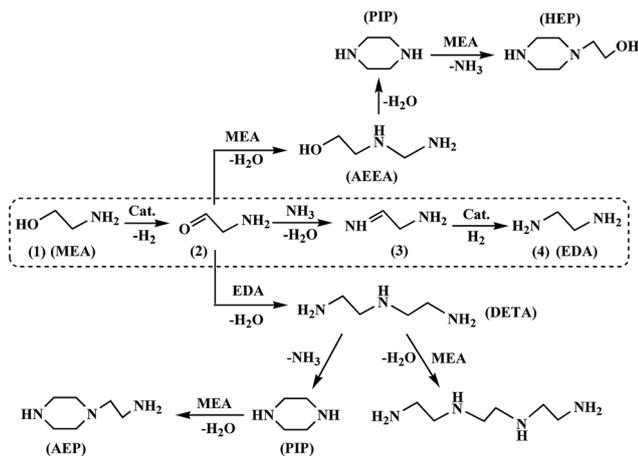
Fig. 1 Reductive amination pathways of MEA.

and aliphatic alcohols. Ni-based catalytic system has proved to be cost-effective and highly active for the amination reaction and has been extensive applied in industry. In one of the representative research, Shimizu and his group have studied the influence of acid–base property and metal particle size of Ni/Al$_2$O$_3$ catalysts on N-alkylation of amines with alcohols.[18,19] They clarified that the coexistence of acidic and basic sites on Al$_2$O$_3$ is indispensable for the reductive amination reaction. Moreover, surface metallic Ni sites are proved to be active sites and the small Ni particles with low-coordinated Ni^0 atoms show higher turnover number during the reaction. The effect of acidity or metallic surface area on the catalytic performance of supported Ni catalyst in other reductive amination reactions has also been reported by researchers.[17,21] Furthermore, for the reductive amination of MEA, many patents have reported that the introduction of Re into the Ni-based catalysts could not only improve the MEA conversion but enhance the selectivity of EDA.[25,26] Although the Ni–Re/Al$_2$O$_3$ catalysts have been applied in industry for decades, studies on the Ni–Re/Al$_2$O$_3$ catalytic system for reductive amination are scarce and presented mainly in the patent literatures. The role of Re promoter on the Ni–Re catalysts is still ambiguous. In order to comprehend the catalytic processes and design novel catalyst with better performance, it is of great significance to study the effect of Re in the Ni–Re catalysts on the behavior for the reductive amination process.

We report herein that Al$_2$O$_3$ supported Ni–Re catalysts act as heterogeneous catalysts for the reductive amination of MEA with ammonia under hydrogen atmosphere in a trickle bed reactor. A series of Ni–Re/Al$_2$O$_3$ catalysts with different loading of Re were prepared by co-impregnating method. Combined with various catalyst characterizations, the physicochemical properties and catalytic performance of Ni–Re/Al$_2$O$_3$ were discussed in detail so as to investigate the role of Re in the catalytic system.

Experimental

Materials and catalysts

All the catalysts were prepared by incipient-wetness impregnation method. The Ni/Al$_2$O$_3$ catalyst with 15 wt% Ni (the mass

ratio of Ni : Al$_2$O$_3$ was 15 : 100) was synthesized by impregnation of Al$_2$O$_3$ (Shandong Aluminum Corp., A-AS-04) with an aqueous solution of Ni(NO$_3$)$_2$·6H$_2$O (99.9% purity). After impregnation, the catalyst was initially dried at room temperature. The dried catalyst was then kept in an oven at 120 °C for 4 h and in a muffle at 500 °C for another 4 h. The calcined catalyst was denoted as Ni15. The monometallic Re/Al$_2$O$_3$ catalyst with 2 wt% Re (the mass ratio of Re : Al$_2$O$_3$ was 2 : 100) was synthesized by impregnation of Al$_2$O$_3$ with an aqueous solution of NH$_4$ReO$_4$ (99.99% purity). The drying and roasting processes were the same as before and the obtained catalyst was denoted as Re2. Ni–Re/Al$_2$O$_3$ catalysts were prepared by co-impregnation of the mixture of Ni(NO$_3$)$_2$·6H$_2$O and NH$_4$ReO$_4$ aqueous solution on Al$_2$O$_3$. The Ni loading was fixed as 15 wt% and the Re loadings were 0.5, 1, 2, and 3 wt%, respectively. The drying and roasting processes were the same as before. The calcined Ni–Re/Al$_2$O$_3$ catalysts were denoted as Ni15–Rex, where x represented the loading of Re. Before reaction, the calcined catalysts were reduced *in situ* for 4 h at 390 or 500 °C in H$_2$ flowing at 100 mL min^{-1}. The reduced catalysts henceforth were designated Ni15–Rex–yR, where y was the reduction temperature.

Catalyst characterization

N$_2$ physisorption was measured at Quantachrome Autosorb-1 instrument. Before measurement, each catalyst was outgassed at 300 °C for 3 h under vacuum. The BET surface area was calculated from the range $P/P_0 = 0.05$–0.30 in the adsorption branch. The total pore volume was determined by the amount of N$_2$ adsorbed at a P/P_0 of 0.99.

Total Ni or Re metal contents in calcined catalysts were determined by inductively coupled plasma optical emission spectroscopy (ICP-OES). Perkin Elmer Optima 7300 DV was applied for elemental detection.

The X-ray diffraction (XRD) analysis of catalysts was performed on a PANalytical X'Pert PRO diffractometer equipped with Cu Kα1 radiation source. The data were recorded with a scan speed of 0.04° s^{-1} and a step size of 0.013°.

Diffuse reflectance UV-vis (DR UV-vis) analysis of the calcined catalysts was performed on a Varian Cary spectrophotometer with BaSO$_4$ used as a reference.

H$_2$-temperature programmed reduction (H$_2$-TPR) was performed on an Altamira Instruments AMI-300 equipped with a thermal conductivity detection (TCD) device. Typically, 100 mg of catalyst was placed in a quartz reactor. Firstly, the sample was pre-treated at 400 °C for 30 min in an Ar flow, followed by cooling to 50 °C. Next, the temperature was raised from 50 °C to 900 °C with a heating rate of 10 °C min^{-1} in a 10% H$_2$/Ar flow (30 mL min^{-1}). The TCD was used to detect the amount of H$_2$ consumption.

Temperature programmed desorption (TPD) experiments of NH$_3$ were conducted using an Altamira Instruments AMI-300 equipped with a thermal conductivity detection (TCD) device. Approximately 100 mg of catalyst was placed in a quartz reactor. Firstly, the catalyst was pre-reduced at 390 °C for 1 h under 10% H$_2$/Ar flow. Next, the catalyst was heated under stream of Ar

at 600 °C for 30 min then cooled to 50 °C. Further, catalyst was exposed to a flow (30 mL min^{-1}) of 5% NH$_3$/Ar for 2 h. After being purged in Ar for 1 h, the catalyst was heated linearly at 10 °C min^{-1} to 600 °C in an Ar flow (30 mL min^{-1}).

CO chemisorption experiments were performed at 50 °C using an Altamira Instruments AMI-300 equipped with thermal conductivity detection (TCD) device. Typically, about 100 mg of catalyst was placed in a quartz reactor. Firstly, the catalyst was heated at 400 °C for 30 min in an Ar flow, followed by *in situ* reduction at 390 or 500 °C for 4 h in a H$_2$ flow. The H$_2$ consumption was detected by TCD. The catalyst was then purged with a He flow of 30 mL min^{-1}, at 400 or 510 °C for 1 h, respectively. The catalyst was cooled to 50 °C and 10% CO/He pulse chemisorption was initiated at 50 °C. The catalyst was then flushed with a He flow of 30 mL min^{-1} for 30 min at 50 °C. Finally, CO-TPD pattern was recorded in the range of 50–800 °C at a heating rate of 10 °C min^{-1} in a He flow (30 mL min^{-1}). The area under the TCD curve below the reduction temperature was used for the calculation of chemisorbed CO volume.[47,48] The Ni metal surface area, dispersion, and Ni metal crystal sizes were calculated using the equations described by Velu *et al.*[49] As a note, the reduction degrees were determined by the ratios of the amounts of H$_2$ consumption during H$_2$-TPR to the theoretical values calculated by ICP-OES measurements. When calculating the reduction degree of Ni in Ni15–Re2 catalyst, the H$_2$ consumption of Re in the Ni15–Re2 catalyst was supposed to be equal to that in Re2 catalyst at the same reduction condition.

The *in situ* X-ray photoelectron spectroscopy (XPS) spectra were recorded using Thermo ESCALAB 250Xi X-ray photoelectron spectrometer. A monochromatic X-ray source of Al Kα of 15 kV was applied. Special regions were Al 2p, Ni 2p and Re 4f. The charging effect was adjusted according to the standard Al 2p line at 74.5 eV.[50] The peak fitting of Ni 2p$_{3/2}$, Re 4f$_{7/2}$, and Al 2p primary peaks were selected for the quantification of surface components. The samples were transferred to the XPS chamber and *in situ* reduced at 500 °C for 2 h under H$_2$ flow. After each reduction, the XPS chamber was evacuated to about 7.1 × 10^{-5} Pa and the XPS measurements were sequentially conducted.

The morphology of the catalysts was investigated by a JSM-7800F scanning electron microscopy (SEM) instrument. The segregation of Ni species was characterized by SEM in back-scattered electron mode.

Transmission electron microscopy (TEM), scanning transmission electron microscopy (STEM), and energy dispersive X-ray (EDX) line scan were acquired with a Tecnai G2 F30 S-Twin electron microscope, operating at 300 kV. The particle size distribution of sample was measured from more than 20 TEM images which obtained at different selected regions.

Materials and catalysts

The details of the reaction method was described in the ESI.† In short, the reductive amination of MEA was carried out in a trickle bed reactor (9 mm inner diameter). About 3.4 mL catalyst (about 2.4 g) was placed in the middle of the reactor and the rest space was filled with about 22 mL silica sand. The raw material consisted of MEA and liquid ammonia. The mole ratio

between MEA : NH$_3$ was 1 : 10. The liquid hourly space velocity (LHSV) of MEA in the reaction was about 0.5 h^{-1}. The H$_2$ flow rate was controlled by mass flowmeter, corresponding to a space velocity of about 60 h^{-1}. Before reaction, the catalysts were *in situ* reduced by pure H$_2$ for 4 h at either 390 or 500 °C. The reductive amination reactions were conducted at 170 °C and 8 MPa. The liquid phase products were collected at 5–11 h reaction intervals. Then, the samples were quantified by gas chromatograph (Agilent 7890) fitted with a flame ionization detector and a DB-35 capillary column, and *N*,*N*-dimethylformamide as an internal standard.

The conversion of MEA and the selectivity of the products were calculated by the equations as follows:

$$\text{Conversion of MEA } (\%) = \frac{n_{\text{MEA,in}} - n_{\text{MEA,out}}}{n_{\text{MEA,in}}} \times 100$$

$$\text{Selectivity of product i } (\%) = \frac{n_i}{\sum n_i} \times 100$$

where $n_{\text{MEA,in}}$ was the moles of MEA initially added, $n_{\text{MEA,out}}$ was the moles of MEA that remained in the products, and n_i was the moles amount of compound i in the products.

Results and discussion

N2 adsorption–desorption

The BET equation was conducted to inspect the porous nature of Al$_2$O$_3$ and Ni-based catalysts. Fig. 2 shows the N$_2$ adsorption–desorption isotherms of calcined Al$_2$O$_3$ support and catalysts. All the isotherms were identified as type IV, which was characteristic of mesoporous materials. The isotherms exhibited type H4 hysteresis loops, indicating the existence of irregular channel systems. The structural properties of support and catalysts, such as surface area, pore volume, and average pore diameter, are shown in Table 1. The BET specific surface area of
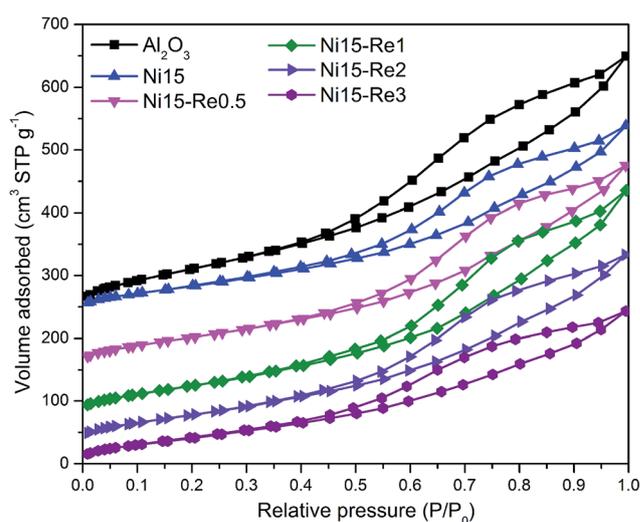
Fig. 2 N$_2$ adsorption–desorption isotherms of Al$_2$O$_3$ support, Ni15, Ni15–Re0.5, Ni15–Re1, Ni15–Re2, and Ni15–Re3 catalysts.

Al_2O_3 support was calculated from N_2 isotherms at -196.6 °C, and was measured as 388.1 m^2 g^{-1}. After modified with Ni or Re, obvious decrease in surface area and pore volume was observed. For Ni–Re doped catalysts, surface area values were in the range of 231–268 m^2 g^{-1}. The reduction of surface area and pore volume after impregnation may be caused by the partial blockage of mesoporous structure by metal species.

XRD

X-ray diffraction experiments (XRD) analysis technique was performed to identify the crystal structure of Al_2O_3 supported Ni and Ni–Re catalysts. As Ni–Re catalysts exhibited similar spectra (Fi. S1†) after calcination, only Ni15 and Ni15–Re2 samples (Fig. 3) were chosen to analyze the crystal structure. Meanwhile, the spectrum of Al_2O_3 support was also shown for comparison. For Al_2O_3 support, the XRD pattern showed the diffraction peaks at $2\theta = 37.6°$, $39.5°$, $45.9°$, and $67.0°$, corresponding to (311), (222), (400), and (440) crystal planes of γ-Al_2O_3 with low crystallinity (JCPDS 29-0063), respectively. For Ni15 catalyst, only weak diffraction line at $2\theta = 42.3°$ originating from bulk NiO (200) crystal plane (JCPDS 44-1159) was detected. In contrast, the NiO diffraction peak at 2θ value of $42.3°$ was not observed on Ni15–Re2 sample, implying the good dispersion of Ni species on the Al_2O_3 surface. Moreover, for Ni15 and Ni15–Re2 catalysts, the broad peak at $66.5°$, which was between the values of $2\theta = 67.0°$ for γ-Al_2O_3 and $2\theta = 65.5°$ for stoichiometric $NiAl_2O_4$ spinel (JCPDS 10-0339), can be indexed to non-stoichiometric $NiAl_2O_4$ phase on the catalysts. It has been reported that Ni species have a tendency to preserve monolayer dispersion and form surface $NiAl_2O_4$-like species on the Al_2O_3 support until the content of Ni is higher than the threshold coverage.[51–54]

The XRD patterns of 390 °C reduced Ni and Ni–Re catalysts are shown in Fig. S1.† There were no significant changes in the diffraction patterns as compared with the calcined samples. The metallic Ni diffraction peaks were not observed, ascribed to the low crystallinity, low reduction degree, or/and small particle size of metallic Ni on the support. For 500 °C reduced Ni15 and Ni15–Re2 catalysts (Fig. 3), diffraction peaks were observed at $2\theta = 44.3°$, $51.7°$, and $76.1°$, corresponding to (111), (200), and (220) crystal planes of metallic Ni (JCPDS 04-0850), respectively. With the use of Scherer's formula, average metallic Ni size of 6.2 nm was found for the Ni15–500R catalyst. However, for Ni15–Re2–500R sample, the intensity of the metallic Ni peaks
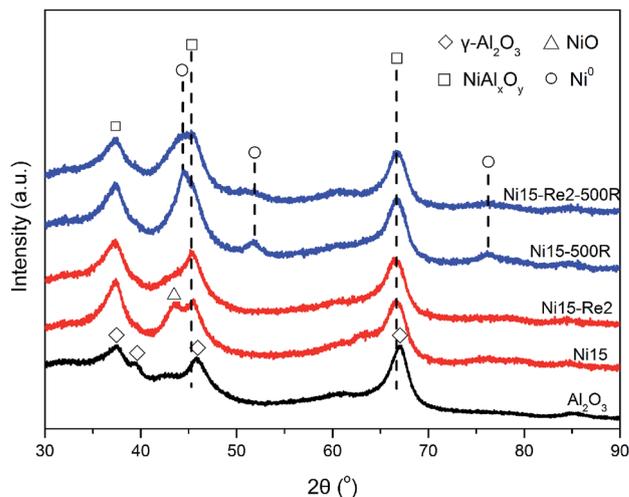

Fig. 3 XRD patterns of Al_2O_3 support, calcined and 500 °C reduced Ni15, Ni15–Re2 catalysts.

was too weak to calculate the metal size, suggesting the high dispersion of metallic Ni phase. Moreover, the diffraction peaks of Re were absent in all XRD patterns of Ni–Re catalysts, because of its lower loading content and weak crystallization, on the other hand, also implying the good dispersion of Re species. On the basis of the analysis results, it could be concluded that the introduction of Re effectively improves the dispersion of Ni species on the γ-Al_2O_3 surface after calcination and reduction treatments.

DR UV-Vis spectroscopy

Diffuse reflectance ultraviolet-visible (DR UV-Vis) spectroscopy was applied to research the symmetry and coordination of Ni species in the catalysts. The reflectance spectra are shown in Fig. 4. It can be observed that the Al_2O_3 and Re2 samples showed no absorption bands in the range of 350–800 nm, while five bands can be observed from the spectrum of the Ni15 catalyst. The band appearing around 377 nm, ascribed to the d–d electron transitions in octahedral Ni^{2+} (Ni[O]), was a fingerprint for NiO lattice.[51] The band at 410 nm was attributed to Ni [O] in surface $NiAl_2O_4$-like spinel.[55] The adsorption bands in the region 550–650 nm as a doublet with maxima at 592 and 638 nm were assigned to the electron transitions of tetrahedral Ni^{2+} (Ni [T]) in bulk $NiAl_2O_4$ lattice. The adsorption band around 713 nm

Table 1 Structural properties of Al_2O_3 support and catalysts

Catalyst	Surface area^a (m^2 g^{-1})	Pore volume^b (mL g^{-1})	Pore diameter^c (nm)	Ni loading^d (wt%)	Re loading^d (wt%)
Al_2O_3	388.1	0.690	5.6	—	—
Ni15	229.7	0.482	6.5	12.5	—
Ni15–Re0.5	268.1	0.536	5.6	12.3	0.3
Ni15–Re1	256.4	0.572	5.7	12.2	0.7
Ni15–Re2	238.3	0.481	6.5	11.7	1.4
Ni15–Re3	231.6	0.408	5.5	11.5	2.2

^{a} Calculated by BET equation. ^{b} BJH desorption pore volume. ^{c} BJH desorption average pore volume. ^{d} Obtained from ICP-OES results.
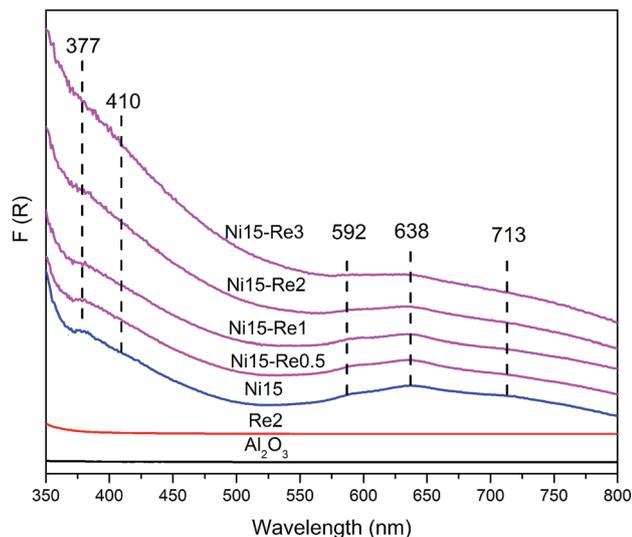
Fig. 4 DR UV-Vis spectra of Al_2O_3 support, Re2, Ni15, Ni15−Re0.5, Ni15−Re1, Ni15−Re2, and Ni15−Re3 catalysts.
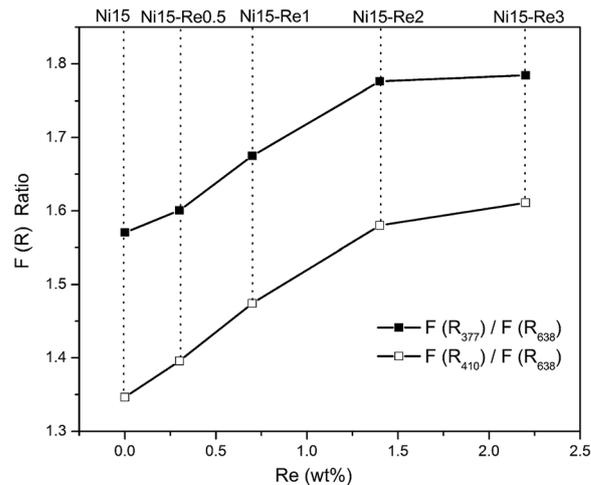

Fig. 5 Variation of the $F(R)$ ratio (the ratio calculated from the Kubelka−Munk functions intensities of the band at 377, 410, and 638 nm) with the Re mass content (ICP-OES results) for Ni and Ni−Re catalysts.

could be assigned to both d–d electron transition of Ni[O] in NiO and Ni[T] in the $NiAl_2O_4$ lattice.[55] When Re was incorporated to the Ni-based catalysts, an increase in the intensity of adsorption bands around 377 and 410 nm was observed. Meanwhile, the intensity of the bands at 592, 638, and 713 nm decreased with increase of Re content. The DR UV-Vis results indicated that more NiO and surface $NiAl_2O_4$-like spinel were generated and the proportion of bulk $NiAl_2O_4$ was reduced on the Ni–Re catalysts. Since the NiO diffraction peaks were not observed for the Ni–Re catalysts in the XRD patterns (Fig. 3), it was reasonable to conclude that the NiO species were highly dispersed on the Re promoted Ni–Re catalysts.

To further analyze the proportion of Ni[O] and Ni[T] in the catalysts, the variation of the Kubelka–Munk function ratio of $F(R_{377})/F(R_{638})$ and $F(R_{410})/F(R_{638})$ with the Re mass content for Ni and Ni–Re catalysts were plotted as a semi-quantitative method. As results shown in Fig. 5, the ratio of $F(R_{377})/F(R_{638})$ and $F(R_{410})/F(R_{638})$ increased with Re content up to about 1.4 wt%, and started to level off with more Re loading. This result indicates that the addition of Re promoter facilitates the conversion of Ni[T] to Ni[O]. In addition, Ni[O] ions were reported to be reduced more easily than Ni[T].[56] The increase of Ni[O] proportion may enhance the reducibility of Ni^{2+} in Ni–Re catalysts. In conclusion, the addition of Re to Ni catalysts generates more Ni[O] species and improves the proportion of NiO and surface $NiAl_2O_4$-like spinel.

H2-TPR

The influence of Re on the reducibility of Ni–Re/Al_2O_3 catalysts was analyzed by H2-TPR measurements and the profiles are shown in Fig. 6. The corresponding H2 consumptions and reduction degrees are listed in Table S1.† For the Ni15 catalyst, three regions of reduction peaks can be observed. The first range at about 350–470 °C can be assigned to the surface bulk-like NiO species which was weakly interacted with Al_2O_3

support; the second range around 470–725 °C could be ascribed to the reduction of surface $NiAl_2O_4$-like spinel, which was highly dispersed on Al_2O_3 support; the third range above 725 °C was attributed to the reduction of bulk $NiAl_2O_4$ spinel, which had a strong interaction with Al_2O_3 support and difficult to be reduced.[51,57] The reduction degree of Ni15 was 92%.

The reduction profile of Re2 sample displayed two reduction peaks at 367 °C and 482 °C, similar to the results reported by Bare et al.[53] The two step reduction of Re2 may be involved in the reduction of different Re valences. The reduction degree of Re2 was calculated to be 85%, indicating rhenium oxide species were incomplete reduced. The average valence of Re was calculated to be about +1. The H2-TPR patterns of Ni–Re catalysts were different from the Ni15 catalyst. The peaks below 470 °C, which could be assigned to reduction of bulk-like NiO or
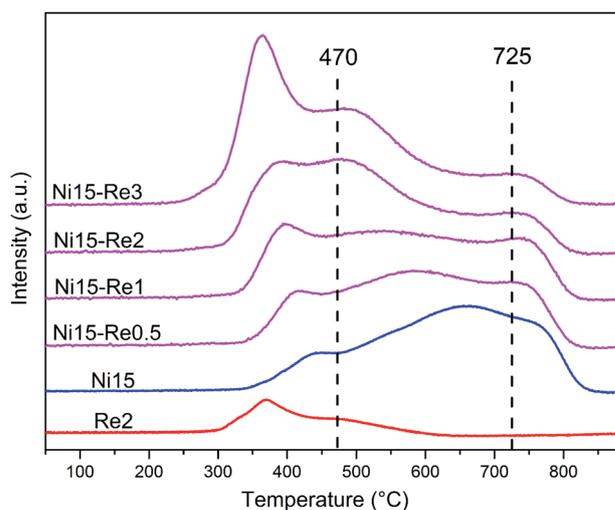

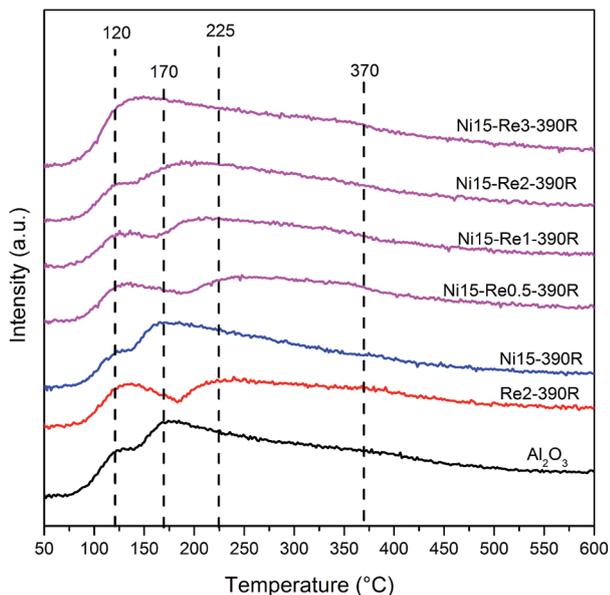Fig. 6 H2-TPR profiles of Re2, Ni15, Ni15−Re0.5, Ni15−Re1, Ni15−Re2, and Ni15−Re3 catalysts.

Fig. 7 NH₃-TPD profiles of Al₂O₃ support, Ni15, Re2, Ni15−Re0.5, Ni15−Re1, Ni15−Re2, and Ni15−Re3 catalysts.

Ni–Re oxide species, shifted to lower temperature and became much stronger as the loading of Re increased from 0.5 to 3 wt%. Moreover, the reduction peaks belonged to surface NiAl$_2$O$_4$-like species (470–725 °C) were shifted toward lower temperature as the increase of Re loading, indicating the addition of Re promoter decreased the reduction temperature of Ni–Re catalysts. Furthermore, as the increase of Re loading, the peaks related to the reduction of bulk NiAl$_2$O$_4$ above 725 °C became much weaker, indicating that the addition of Re can prevent the diffusion of Ni^{2+} into the Al$_2$O$_3$ lattice to form NiAl$_2$O$_4$ specie,

which is hardly reduced and inert for the amination reaction.[21] The reduction degrees for Ni–Re/Al$_2$O$_3$ catalysts were around 95%. In conclusion, H$_2$-TPR studies suggest that the introduction of Re significantly improves the reducibility of Ni–Re catalysts and inhibits the formation of bulk NiAl$_2$O$_4$ species.

Acid–base properties

As both the acidic and basic nature of the catalysts were reported to be necessary for the reductive amination reaction,[18,19] NH$_3$-TPD, CO$_2$-TPD, and PY-IR experiments were conducted to investigate the acid–base character of catalysts. The NH$_3$-TPD profiles are shown in Fig. 7. The spectrum of Al$_2$O$_3$ support showed a doublet at 120 and 170 °C. The peak at 120 °C could be attributed to desorption of residual physically absorbed NH$_3$. The second peak at 170 °C was assigned to chemisorb NH$_3$ from weak acidic sites. For Al$_2$O$_3$ supported Re sample, desorption peak at 170 °C shifted up to about 225 °C, indicating the presence of Re enhanced the acid strength of Al$_2$O$_3$ support. The NH$_3$-TPD profile of Ni15 catalyst was similar to the Al$_2$O$_3$ support profile. After modified with Re, Ni–Re catalysts exhibited a broad peak in the range of 225–370 °C, indicating the introduction of Re improves the acid strength of Ni–Re catalysts. Moreover, the intensity of desorption peak around 170 °C increases with the increase of Re loading in Ni–Re catalysts.

The pyridine adsorption infrared (IR) spectra (Fig. S2†) demonstrate that Al$_2$O$_3$ support mainly contains surface Lewis acid sites. The impregnation of Ni or Re to the Al$_2$O$_3$ support doesn't affect the type of acidic centers. Furthermore, the basic contents measured from the CO$_2$-TPD results (Fig. S3 and Table S2†) indicate that few basic sites exist on the Al$_2$O$_3$ support and the impregnation of Ni or Re species has little impact on the base character of the catalysts.
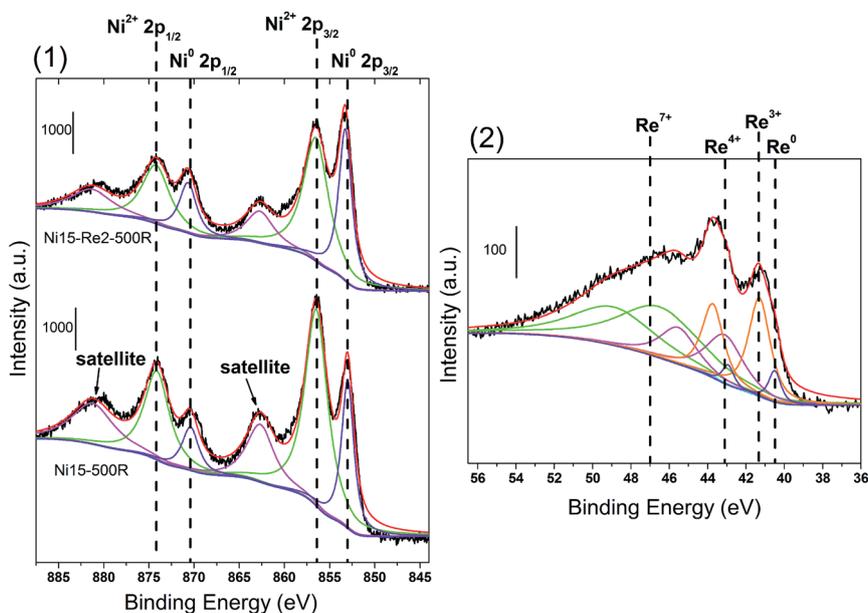

Fig. 8 *In situ* XPS of (1) Ni 2p region for Ni15−500R and Ni15−Re2−500R catalysts, and (2) Re 4f region for Ni15−Re2−500R catalyst. The dash lines in the spectra correspond to the Ni 2P or Re 4f$_{7/2}$ peaks of different valance states.

Table 2 Binding energies and atomic ratios for 500 °C reduced Ni15 and Ni15–Re2 catalysts

Catalyst	Ni 2P$_{3/2}$^{a} (eV)		Ni 2P$_{1/2}$^{a} (eV)		Atomic ratio Ni/Al	Re 4f$_{7/2}$^{a} (eV)				Atomic ratio Re/Ni
	Ni^{2+}	Ni^0	Ni^{2+}	Ni^0		Re^0	Re^{3+}	Re^{4+}	Re^{7+}	
Ni15–500R	856.5 (70.9)	853.0 (29.1)	874.1	870.4	0.0725	—	—	—	—	—
Ni15–Re2–500R	856.5 (60.9)	853.3 (39.1)	874.2	870.6	0.0678	40.5 (4.6)	41.3 (25.1)	43.1 (21.0)	46.5 (49.3)	0.0836

^{a} BEs of Ni 2P or Re 4f$_{7/2}$ species. The percentages of Ni or Re with different valance states are shown in parentheses.

In situ XPS

In situ X-ray photoelectron spectroscopy (XPS) was used to analyze the valance state of the elements and the surface composition in the 500 °C reduced Ni15 and Ni15–Re2 catalysts. Fig. 8 presents the XPS spectra of Ni 2p and Re 4f regions from the Ni15–500R and Ni15–Re2–500R samples. The curve fitting results of Ni 2p and Re 4f$_{7/2}$ are listed in Table 2. The Ni15–500R catalyst had two main peaks at 853.0 and 870.4 eV, corresponding to the Ni^0 2p$_{3/2}$ and Ni^0 2p$_{1/2}$, respectively. Moreover, the presence of peaks at 856.5 and 874.1 eV, respectively corresponding to the BEs of Ni^{2+} 2p$_{3/2}$ and Ni^{2+} 2p$_{1/2}$, indicating the Ni species in the Ni15 catalyst were partially reduced. The peaks at 862.7 eV and 881.2 eV were ascribed to the shake-up satellite peaks of Ni^{2+} 2p$_{3/2}$ and Ni^{2+} 2p$_{1/2}$, respectively.[50,51,59] It was notable that the BE of Ni^{2+} 2p$_{3/2}$ at 856.5 eV was higher than that of published bulk NiO species (around 854.5 eV), indicating the presence of NiAl$_2$O$_4$ species on the catalyst surface.[50] For Ni15–Re2–500R catalyst, the peak intensity of Ni^0 2p$_{3/2}$ and Ni^0 2p$_{1/2}$ was higher than the case in Ni15–500R catalyst. According to the calculation results in Table 2, the reduction degree of Ni15–500R catalyst was 29.1%, while that of Ni15–Re2–500R catalyst increased to 39.1%, indicating the presence of Re enhanced the reducibility of Ni species. Furthermore, from curve fitting results, the BE of Ni^0 2p$_{3/2}$ in Ni15–Re2–500R was 0.3 eV higher than that in Ni15–500R catalyst. Chayakul *et al.* have reported that d-band electron densities of Ni could be reduced by the electron transformation from Ni to Re.[58] The shift in BEs of Ni^0 2p$_{3/2}$ when comparing Ni15–500R and Ni15–Re2–500R provided evidence of an interaction between Ni to Re species. In addition, the surface Ni/Al ratios of catalysts were in the range of 0.0678 to 0.0725, which were lower than the theoretical value of 0.122, because of the incorporation of Ni^{2+} into the Al$_2$O$_3$ lattice by the strong interaction between the surface Ni and Al$_2$O$_3$ support. In conclusion, the XPS results proved that the addition of Re promotes the reduction of Ni^{2+} compounds and electron interaction existed between Ni and Re.

The XPS spectrum of Re 4f for the Ni15–Re2–500R catalyst is shown in Fig. 8(2). The separation of the spin–orbit Re 4f$_{7/2}$–4f$_{5/2}$ doublet were fixed for the curve fitting of Re spectra. Four valance states of Re were selected to get the best fitting. The deconvoluted peaks at 40.5, 41.3, 43.1, and 46.5 eV were corresponded to the 4f$_{7/2}$ BEs of Re^0, Re^{3+}, Re^{4+}, and Re^{7+} components, respectively.[60–62] The concentration of Re^{x+} species was calculated by the intensity of Re 4f$_{7/2}$ and shown in Table 2. The reduction degree and average valence of Re were calculated to be about 30% and +5, respectively. The results indicated that

the major Re species existed as a mixture of various oxidation states after reduction at 500 °C. These multiple oxidation states after reduction might arise from the strong oxophilicity of Re species. Bare *et al.* have studied the oxidized and reduced states of Re over Re/Al$_2$O$_3$ using a combination of X-ray absorption fine structure (XAFS) and theoretical approaches.[53] They concluded that the oxidized Re species still existed even after reduction at 700 °C under dry H$_2$. Furthermore, for Ni15–Re2–500R catalyst, the surface atomic ratio of Re/Ni was found to be 0.0836, which was much higher than the theoretical value calculated by ICP-OES (0.0377). This result indicates the enrichment of Re species on the surface of Ni–Re/Al$_2$O$_3$ catalysts.

BSE-SEM and CO-adsorption

The dispersion of metal particles for the reduced Ni15 and Ni15–Re2 catalysts at different temperature were further examined by SEM in backscattered electron (BSE) image mode. The images are shown in Fig. 9. It should be noted that BSE image was used to detect differences in the atomic number within the catalysts. The contrast between particles and support was mainly linked to the atomic masses or atomic numbers of the corresponding elements. For the Ni15–390R sample (Fig. 9(1)), Ni containing particles with an average size of about 8 nm were observed on the surface of catalyst. When the reduction temperature was increased to 500 °C (Fig. 9(2)), more Ni particles were detected on the sample and the particle sizes slightly increased to about 10 nm, indicating the aggregation of Ni under higher reduction temperature. For Re promoted Ni15–Re2 catalyst (Fig. 9(3 and 4)), the particle sizes were mostly
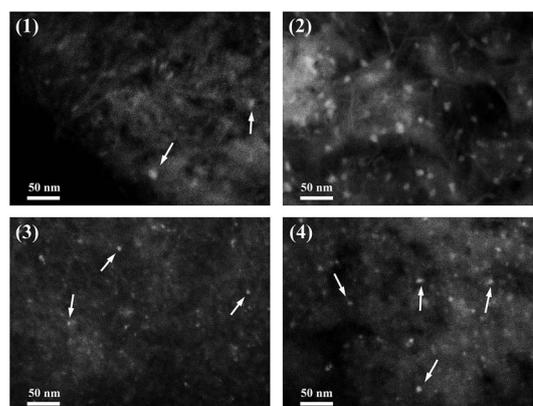

Fig. 9 BSE-SEM images of the reduced catalysts: (1) Ni15–390R, (2) Ni15–500R, (3) Ni15–Re2–390R, and (4) Ni15–Re2–500R.

Paper

Table 3 Ni particle sizes and dispersions measured by CO chemisorption and reduction degree

Catalyst	Reduction temperature (°C)	Reduction degree (%)	CO uptake (μmol $g_{cat.}^{-1}$)	Ni^0 surface area (m^2 $g_{cat.}^{-1}$)	Ni^0 dispersion (%)	Ni^0 crystal size (nm)
Ni15	390	Ni-8.8	17.4	0.7	9.3	19.4
	500	Ni-27.3	56.1	2.2	9.6	18.7
Ni15–Re2	390	Ni-24.8	77.6	3.0	15.7	11.5
	500	Ni-50.9	125.3	4.9	12.4	14.5
Re2	390	Re-47.7	—	—	—	—
	500	Re-72.8	—	—	—	—

around 4 and 6 nm after reduced at 390 and 500 °C, respectively. The particle sizes of reduced Ni15–Re2 catalysts were much smaller than those of reduced Ni15 catalysts, indicating the addition of Re promoter effectively improved the dispersion of Ni after reduction.

For supported Ni catalysts, metallic Ni sites had proved to be active species for the dehydrogenation–hydrogenation steps. CO-TPD measurement was applied to study the influence of Re promoter on the metallic Ni site, metal dispersion, and average Ni particle size of the Ni based catalyst. Ni15 and Ni15–Re2 catalysts were chosen for comparison. The CO uptakes and analogy computation results, corrected by the reduction degrees, are summarized in Table 3. The CO uptake results indicated that a trace amount CO was adsorbed on the surface of Re2 catalyst. Moreover, since CO adsorption infrared (IR) spectra (Fig. S4†) proved that major CO species were linearly adsorbed on the surface of Ni^0 sites, the Ni : CO ratio in chemisorption was taken as 1 to calculate the Ni^0 surface area.[47] As shown in Table 3, after modified with Re promoter, the Ni^0 surface areas of the 390 and 500 °C reduced catalysts increased from 0.7 to 3.0 m^2 $g_{cat.}^{-1}$ and 2.2 to 4.9 m^2 $g_{cat.}^{-1}$, respectively. Furthermore, Re promoted Ni15–Re2 catalyst showed higher dispersion and smaller particle size in comparison with the monometallic Ni15 catalyst after reduction.

It should be noted that the Ni^0 particle sizes obtained from previous XRD or BSE-SEM methods were smaller than those

calculated from CO uptakes. This difference might arise from the decoration of Ni particles with $NiAl_2O_4$ species after reduction. The aluminate shells on the surface of metallic Ni particles might prevent the adsorption of CO gas, resulting in low CO uptake. Salagre *et al.* have concluded that Ni crystallites surface would be decorated with porous $NiAl_2O_4$ species during reduction process.[63] A similar model of $NiAl_2O_4$ structure after reduction was proposed by Jerzy earlier.[64] This speculation was further supported by the XRD, H_2-TPR, and XPS analyses which showed that Ni species mainly existed as surface $NiAl_2O_4$ spinel in the catalyst. According to the CO-adsorption results, the addition of Re in the Ni based catalysts significantly improves the Ni dispersion and generates more Ni^0 sites after reduction.

Reductive amination of MEA

Reductive amination of MEA was carried out in a trickle bed reactor. The amine products collected after reaction about 12 h were analyzed and summarized in Table 4. Interestingly, it was found that Ni15–Re*x* catalysts could efficiently catalyze the reductive amination of MEA to EAD. The conversion and EDA selectivity increased to 36.6% and 63.0% (entry 5 in Table 4) with Re content up 2 wt% (Ni–15–Re2–390R), and started to level off with more Re loading (entry 6 in Table 4). In comparison, a very low conversion (7.6%) and EDA selectivity (40.0%) were observed on Ni15–390R catalyst (entry 2 in Table 4), and no detectable activity was observed on Re2–390R catalyst under the

Table 4 Catalytic results for the reductive amination of MEA

Entry	Catalyst	Conversion (%)	Selectivity (%)				
			EDA[a]	AEEA[b]	PIP[c]	DETA[d]	Others[e]
1	Re2–390R	—	—	—	—	—	—
2	Ni15–390R	7.6	40.0	56.2	3.2	0.0	0.6
3	Ni15–Re0.5–390R	22.3	55.6	32.2	5.8	4.3	2.1
4	Ni15–Re1–390R	27.6	60.3	26.2	6.4	4.6	2.5
5	Ni15–Re2–390R	36.6	63.0	20.4	8.1	5.7	2.8
6	Ni15–Re3–390R	37.6	63.6	19.2	8.9	5.2	3.1
7	Ni15–500R	14.5	46.3	37.4	8.5	5.1	2.7
8	Ni15–Re2–500R	43.2	67.7	16.4	8.2	5.5	2.2
9	Ni–Re/Al_2O_3[f]	45.4	69.1	12.9	6.6	10.5	0.9
10	Ni–Re/SiO_2–Al_2O_3[g]	53.0	82.4	9.8	1.1	5.9	0.8
11	Ni15–Re/Al_2O_3[h]	50.4	82.1	4.4	5.1	7.7	0.8

[a] Ethylenediamine. [b] Aminoethylethanolamine. [c] Piperazine. [d] Diethylenetriamine. [e] N-(2-Hydroxyethyl)piperazine and N-Aminoethylpiperazine. [f] Patent (US 5750790):[26] 170 °C, 12.5 MPa, MEA : NH_3 = 1 : 10. [g] Patent (US 6534441 B1):[27] 160 °C, 20.0 MPa, MEA : NH_3 = 1 : 10. [h] The pilot-scale results of our Ni–Re/Al_2O_3 catalysts: 175 °C, 17.5 MPa, MEA : NH_3 = 1 : 10.

same reaction conditions (entry 1 in Table 4). The big difference between Ni15–Rex catalysts and Ni15 catalyst revealed that the presence of Re was critical for reductive amination. The addition of Re not only significantly improved the activity of Ni-based catalysts but also enhanced the selectivity of desired amines, such as EDA and PIP. In consideration of many parallel reactions during reductive amination processes of MEA, the enhancement of the EDA yield was essential to avoid the difficulty during products separating.

The TOF of Ni–Re catalysts (Table S3†) with varied Re loading were estimated for reference according to the method reported by Shimizu.[19] The TOF increases from 213 to 251 h^{-1} with increasing the Re loading from 0.5 to 2 wt% and starts to level off with further increasing Re loading.

In order to compare the activity of Ni15 and Ni15–Re2 catalysts further, we increased the reduction temperature of Ni15 and Ni15–Re2 catalysts from 390 to 500 °C and the results are list in Table 4. The MEA conversion for the Ni15–500R catalyst was still low and product distribution changed little (entry 7 in Table 4). In contrast, the yield of EDA was further improved over the Ni15–Re2–500R catalyst (entry 8 in Table 4). Fig. 10 shows the stability of Ni15–500R and Ni15–Re2–500R catalysts. The results showed that the increase in reduction temperature could increase the initial activity of catalysts. However, for Ni15–500R catalyst, the MEA conversion decreased rapidly with reaction time and nearly deactivated within 23 h. The EDA selectivity declined and the by-product AEEA significantly increased as the activity dropped. For Ni15–Re2–500R catalysts, a slightly decrease of conversion was also observed, but the catalysts performance could reach steady state and maintain a higher

activity. The above results indicate that the addition of Re not only improves the yield of EDA but also inhibits the deactivation during the reductive amination process. In combination with the previously CO chemisorption results, the highly Ni^0 surface area could correspond to the enhancement in the yield of EDA.

Currently, the reports about MEA reductive amination were presented mainly in the patent literatures.[26,27,65] The reaction results of Ni–Re catalysts reported by others were listed in Table 4 (entry 9 and 10). It should be noted that most of patent reported experiments and industrial processes were carried out under high reaction pressure (12–25 MPa). Fischer et al. have reported that ammonia would form a supercritical fluid (critical data of ammonia: $T_c = 132.4$ °C, $P_c = 11.48$ MPa) in a fix-bed reactor under high pressure.[9,10] The formation of supercritical ammonia is crucial to improve the selectivity of primary diamines. Unfortunately, our reaction pressure should not exceed 8 MPa due to the limitations of experimental conditions. In our subsequent pilot-scale study (entry 11), 50.4 percent conversion could be achieved with a selectivity of 82.1 percent for EDA at 175 °C under 17.5 MPa.

Characterization of the spent catalysts

XRD technique was used to investigate the crystalline structure and morphology of the spent Ni15–500R and Ni15–Re2–500R catalysts. XRD patterns are shown in Fig. 11. Both the spent catalysts exhibited obvious diffraction lines at $2\theta = 44.3°$, $51.7°$, and $76.1°$, characteristic of the metallic Ni phase. Average Ni^0 particle sizes of 21.3 and 15.8 nm were found for the spent Ni15–500R and Ni15–Re2–500R catalysts with the use of Scherrer's equation, respectively. Combined with the previous XRD patterns in Fig. 3, it was clear that aggregation and growth of Ni^0 particles occurred during the reductive amination process.

The TEM micrographs and size distributions of Ni^0 particles of spent catalysts are shown in Fig. 12. It was found that Ni particles for the spent Ni15–500R catalyst (Fig. 12(1 and 2)) were heterogeneously dispersed and had a broad distribution of 40 to 550 nm. In addition, large Ni particles with sizes above 1 μm
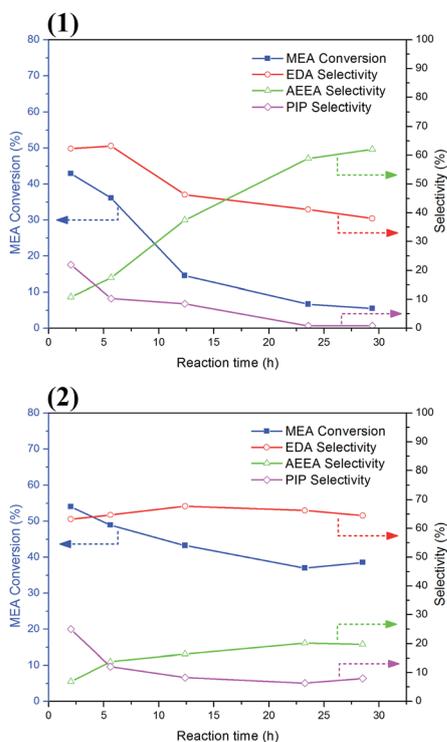
Fig. 10   Stability of (1) Ni15–500R and (2) Ni15–Re2–500R catalysts.
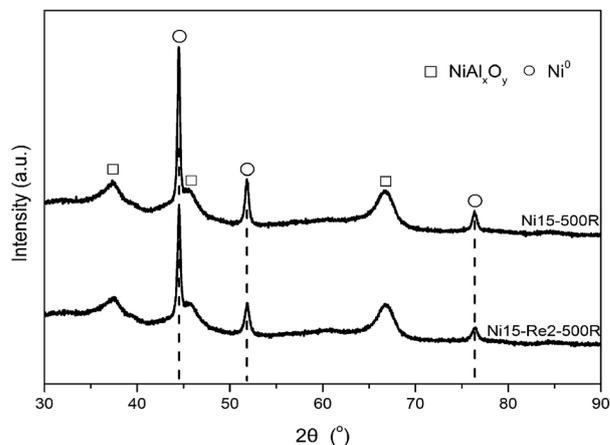
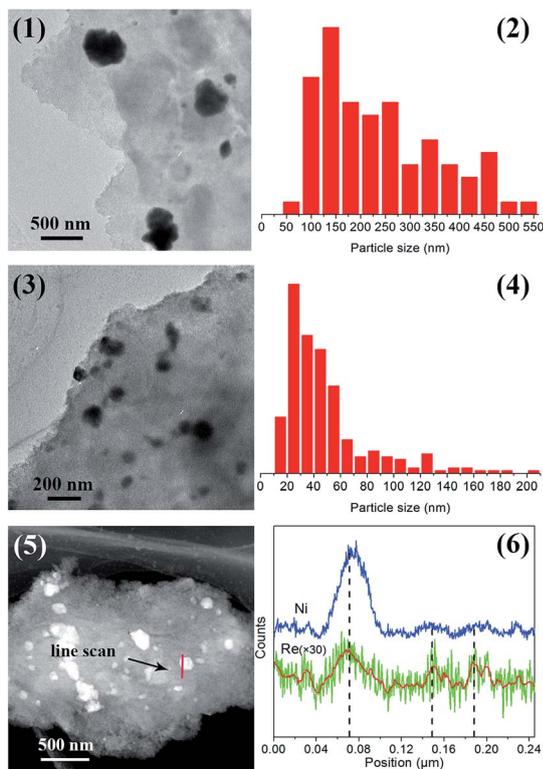Fig. 11   XRD patterns of spent Ni15–500R and Ni15–Re2–500R catalysts.

Fig. 12 TEM images and particle size distributions of: (1) and (2) spent Ni15–500R; (3) and (4) spent Ni15–Re2–500R. (5) STEM image of spent Ni15–Re2–500R, and (6) EDX line scans across a large particle as dedicated by the red line.

were often observed from the TEM images at some selected regions (Fig. S5†). The TEM results clearly indicated that serious sintering of Ni^0 particles happened during reaction for Ni15 catalyst. On the contrary, the Ni^0 sintering process was effectively suppressed in the presence of Re promoter. For spent Ni15–Re2–500R catalyst (Fig. 12(3 and 4)), Ni^0 particles more uniformly dispersed and the sizes of Ni^0 particles densely distributed in a range of 10–60 nm. One should be noted that the difference between the XRD and TEM results was due to the low crystalline of Ni^0 or the sizes of metal particles beyond the applicable scope of Scherrer's equation. The elemental distribution of Ni and Re for spent Ni15–Re2–500R catalyst was examined by STEM-EDX line scan. As shown in Fig. 12(5 and 6), similar trend was observed for the Ni and Re elements in the spent catalysts. The EDX line scan results suggest that the surface of Ni^0 particles is rich in Re species.

Discussion

As indicated by characterization results, the addition of Re promoter affects the structure and activity of Ni/Al_2O_3 catalysts during preparation process and MEA reductive amination. For calcined catalysts, XRD and DR UV-Vis results indicate that most of Ni species existed in the form of non-stoichiometric $NiAl_2O_4$ phase in Ni/Al_2O_3 catalyst. The presence of bulk NiO phase is also detected by XRD. The introduction of Re effectively

enhances the NiO dispersion and facilitates the generation of surface Ni[O] species in $Ni–Re/Al_2O_3$ catalysts.

After reduction, H_2-TPR and *in situ* XPS results show that Re promoter significantly improves the reducibility of Ni. Moreover, as indicated by BSE-SEM and CO-adsorption results, Re promoted Ni/Al_2O_3 catalysts have smaller Ni^0 particle size and more surface Ni^0 sites compared with monometallic Ni/Al_2O_3 catalyst. The enhancement of the Ni reducibility could be explained by two reasons. Firstly, as indicated by DR UV-Vis results, the increase of surface NiO species and Ni[O] proportion for Ni–Re catalysts makes the Ni^{2+} species more easily to be reduced; secondly, the reduction of Ni^{2+} may be accelerated by hydrogen spillover effects on Re atoms. It has been reported that Re could promote the reduction of Co^{2+} or Ce^{4+} species by hydrogen spillover.[59,66] Moreover, both H_2-TPR and *in situ* XPS results indicate that Re species are incomplete reduced and exhibit a mixture of various oxidation states after reduction. Furthermore, the acidity–basicity measurement results suggest that the addition of Re improves the acid strength of catalysts. The generation of new acid sites in bimetallic catalysts comprised of noble metals and oxophilic metal promoters has been reported in recent years.[67,68] Some research reported that the acid–base pair sites adjacent to the Ni^0 sites assisted important steps such as deprotonation of alcohol or hydrogen transfer.[18,19] The enhancement of acidic strength might accelerate the deprotonation of MEA or hydrogen transfer steps.

The characterization results of spent catalysts indicate that Ni/Al_2O_3 catalyst suffers from serious Ni sintering during reaction. The sintering of Ni particles on Al_2O_3 support in the presence of NH_3 and H_2 has been reported by Lif *et al.*[69] They concluded that the presence of NH_3 accelerates the rate of sintering by weakening the interaction between Ni particle and Al_2O_3 support. For Re modified $Ni–Re/Al_2O_3$ catalysts, the Ni sintering process could be effectively suppressed. Moreover, monometallic Re2 catalyst has proved to be inactive during reaction. The reductive amination process is mainly catalyzed by Ni^0 sites. In combination with the reaction and characterization results of spent catalysts, the decline of activity could be ascribed to the sintering of Ni particles during reaction. As shown in Fig. 10(1) (Ni–500R), the MEA conversion drops by a dramatic 86 percent after reaction for about 30 h, compared to the sampling result at 2 h. Meanwhile, serious Ni sintering is observed from the TEM images of spent Ni–500R sample. For Ni15–Re2–500R catalyst (Fig. 10(2)), the MEA conversion decreases from 54% (2 h) to 38% (28 h) with the growth in Ni particle size. Even more interestingly, for both catalysts, the selectivity of products changes along with the catalyst activity. In the initial period, the selectivities of EDA and PIP are higher and selectivity of by-product AEEA is less than 10%. As the MEA conversion decreases to about 36%, the PIP selectivity decreased and more AEEA generated. Along with further decrease of activity, a sharp rise in AEEA selectivity is detected and EDA selectivity decreases to about only 38%. This phenomenon could be explained by the continuous reaction during MEA reductive amination. As shown in Fig. 1, PIP is mainly generated from the amination of AEEA. For high active catalysts, there are sufficient Ni^0 sites on the surface of catalysts

and AEEA would proceed to generate PIP. With sintering of Ni particles during reaction, the amount of surface Ni^0 sites would decline and AEEA selectivity starts to increase. Moreover, competitive reaction between MEA of NH_3 and MEA molecules is in existence during reductive amination and the generation of side product AEEA is inevitable. The reaction results indicate that highly active $Ni–Re/Al_2O_3$ catalyst is beneficial to enhance the selectivities of EDA and PIP and reduce the generation of by-product AEEA.

The interaction between Ni and Re has been confirmed in recent years. Liu *et al.* studied the TiO_2 supported Ni–Re catalysts for selective hydrogenation of methyl esters.[70] Their XPS results suggested that surface enrichment of metallic Re species in bimetallic Ni–Re catalysts caused the enhancement of activity. Gebrestadik *et al.* investigated ReO_x modified Ni catalysts for the hydrogenolysis of glycidol.[71] According to the XPS results, they concluded that Re was decorated by Ni and the collaborative effect between ReO_x and Ni particles was beneficial for the production of 1,3-PD. Yang *et al.* also reported the formation of surface Ni–Re alloy on the $Ni–Re/SiO_2$ catalysts.[67] Furthermore, they suggested that oxophilic Re played a crucial role for the adsorption of O atom during reaction. In our research, the XPS and STEM-EDX line scan results indicated the electron transformation from Ni to Re and the enrichment of Re species on the Ni^0 particles surface. It was reasonable to speculate that surface of Ni^0 particles was decorated with ReO_x species. The collaboration effect between $Ni–ReO_x$ may has an influence on the mechanism of MEA reductive amination. This speculation will be studied in our further study.

Conclusions

The Al_2O_3 supported Ni and Ni–Re catalysts were prepared by impregnation method and evaluated for the reductive amination of MEA in a trickle bed reactor. The $Ni–Re/Al_2O_3$ catalysts showed high activity, high EDA selectivity, and outstanding stability in comparison with the monometallic Ni/Al_2O_3 catalyst. The addition of Re promoter improved Ni dispersion and proportion of Ni[O] species on the surface of $Ni–Re/Al_2O_3$ catalysts. The reducibility of Ni species was significantly improved by the Re promoter. After reduction, $Ni–Re/Al_2O_3$ catalysts exhibited smaller Ni particle size (4–6 nm) and more Ni^0 sites as compared to Ni/Al_2O_3 catalysts. Moreover, the presence of Re improved the acid strength of catalysts. *In situ* XPS and STEM-EDX line scan results indicated that Re species had a mixture of various oxidation states and tended to aggregate on the surface of Ni^0 particles after reduction. The adjacent $Ni^0–ReO_x$ sites might facilitate the dehydrogenation step of MEA. The analysis results indicated that the deactivation of Ni/Al_2O_3 catalyst was mainly caused by the aggregation of Ni^0 particles during reaction. For $Ni–Re/Al_2O_3$ catalysts, the Ni^0 particles were stabilized and sintering process was effectively suppressed by the presence of Re promoter. We concluded that the abundant Ni^0 sites, which combined with good stability of Ni^0 particles and synergic effect of Ni–Re, corresponded to the excellent catalytic performance of $Ni–Re/Al_2O_3$ catalysts.

Conflicts of interest

There are no conflicts to declare.

Acknowledgements

Notes and references

1 G. F. Mackenzie, *US Pat.*, 2 861 995, The Dow Chemical Company, 1958.
2 F. Weiss and R. Lichtenberger, *US Pat.*, 3 068 290, Societe d'Electro-Chimie d'Electro-Metallurgie et des Acieries Electriques d'Ugine, 1962.
3 P. H. Moss and N. B. Godfrey, *US Pat.*, 3 151 115, Jefferson Chemical Company, 1964.
4 J. Johansson and J. Tornquist, *US Pat.*, 3 766 184, Sweden No Drawing Company, 1973.
5 J. Pašek, P. Kondelik and P. Richter, *Ind. Eng. Chem. Prod. Res. Dev.*, 1972, **11**, 333.
6 A. Baiker and W. Richarz, *Ind. Eng. Chem. Prod. Res. Dev.*, 1977, **16**, 261.
7 C. M. Barnes and H. F. Rase, *Ind. Eng. Chem. Prod. Res. Dev.*, 1981, **20**, 399.
8 A. Baiker and J. Kijenski, *Catal. Rev.*, 1985, **27**, 653.
9 A. Fischer, T. Mallat and A. Baiker, *Angew. Chem., Int. Ed.*, 1999, **38**, 351.
10 A. Fischer, T. Mallat and A. Baiker, *J. Catal.*, 1999, **182**, 289.
11 A. Fischer, M. Maciejewski, T. Bürgi, T. Mallat and A. Baiker, *J. Catal.*, 1999, **183**, 373.
12 S. Imm, S. Bähn, L. Neubert, H. Neumann and P. M. Beller, *Angew. Chem., Int. Ed.*, 2010, **49**(8126), 8129.
13 K. O. Marichev and J. M. Takacs, *ACS Catal.*, 2016, **6**, 2205.
14 G. Liang, A. Wang, L. Li, G. Xu, N. Yan and T. Zhang, *Angew. Chem., Int. Ed.*, 2017, **56**, 3050.
15 H. Kimura, *Catal. Rev.*, 2011, **53**, 1.
16 Y. Zhang, G. Bai, X. Yan, Y. Li, T. Zeng, J. Wang, H. Wang, J. Xing, D. Luan and X. Tang, *Catal. Commun.*, 2007, **8**, 1102.
17 J. M. Jehng and C. M. Chen, *Catal. Lett.*, 2001, **77**, 147.
18 K. I. Shimizu, K. Kon, W. Onodera, H. Yamazaki and J. N. Kondo, *ACS Catal.*, 2012, **3**, 112.
19 K. I. Shimizu, N. Imaiida, K. Kon, S. M. A. H. Siddiki and A. Satsuma, *ACS Catal.*, 2013, **3**, 998.
20 J. H. Cho, J. H. Park, T. Chang, G. Seo and C. Shin, *Appl. Catal., A*, 2012, **417**, 313.
21 J. H. Cho, J. Park, T. Chang, J. Kim and C. Shin, *Catal. Lett.*, 2013, **143**, 1319.
22 A. Baiker, D. Monti and S. F. Yuan, *J. Catal.*, 1984, **88**, 81.
23 K. I. Shimizu, S. Kanno, K. Kon, S. Siddiki, H. Tanaka and Y. Sakata, *Catal. Today*, 2014, **232**, 134.
24 J. H. Cho, S. H. An, T. S. Chang and C. H. Shin, *Catal. Lett.*, 2016, **146**, 811.

25 D. C. Best, *US Pat.*, 4 123 462, Union Carbide Corporation, 1978.

26 S. W. King, *US Pat.*, 5 750 790, Union Carbide Corporation & Plastics Technology Corporation, 1998.

27 W. J. Bartley, R. G. Cook, K. E. Curry and S. K. Mierau, *US Pat.*, 6 534 441, Union Carbide Corporation & Plastics Technology Corporation, 2003.

28 Z. Pan, Y. Ding, D. Jiang, X. Li, G. Jiao and H. Luo, *Appl. Catal., A*, 2007, **330**, 43.

29 L. Yan, Y. J. Ding, Y. Lv, X. B. Cheng and L. X. Ma, WO Patent 2013152548 A1, Dalian Institute of Chemical Physics, Chinese Academy of Sciences, 2013.

30 G. Jenzer, T. Mallat and A. Baiker, *Catal. Lett.*, 1999, **61**, 111.

31 L. Zhang, C. Yang, Q. Yao, Y. Hou, Q. Lu and J. Xu, *Mater. Manuf. Processes*, 2014, **29**, 738.

32 J. Runeberg, A. Baiker and J. Kijenski, *Appl. Catal.*, 1985, **17**, 309.

33 W. Hammerschmidt, A. Baiker, A. Wokaun and W. Fluhr, *Appl. Catal.*, 1986, **20**, 305.

34 J. Kijeński, P. J. Niedzielski and A. Baiker, *Appl. Catal.*, 1989, **53**, 107.

35 P. R. Likhar, R. Arundhathi, M. L. Kantam and P. S. Prathima, *Eur. J. Org. Chem.*, 2009, **31**, 5383.

36 T. Yan, B. L. Feringa and K. Barta, *ACS Catal.*, 2015, **6**, 381.

37 H. J. Pan, W. N. Teng and Y. Zhao, *Chem. Commun.*, 2015, **51**, 11907.

38 B. Emayavaramban, M. Roy and B. Sundararaju, *Chem.–Eur. J.*, 2016, **22**, 3952.

39 T. Takanashi, Y. Nakagawa and K. Tomishige, *Chem. Lett.*, 2014, **43**, 822.

40 A. Abdukader, H. M. Jin, Y. X. Cheng and C. J. Zhu, *Tetrahedron Lett.*, 2014, **55**, 4172.

41 X. Xie and V. H. Han, *ACS Catal.*, 2015, **5**, 4143.

42 J. G. Donaire, M. Ernst, O. Trapp and T. Schaub, *Adv. Synth. Catal.*, 2016, **358**, 358.

43 K. K. Wu, W. He, C. Sun and Z. Yu, *Tetrahedron*, 2016, **72**, 8516.

44 Y. Nakamura, K. Kon, A. S. Touchy, K. Shimizu and W. Ueda, *ChemCatChem*, 2015, **7**, 921.

45 S. Siddiki, K. Kon and K. Shimizu, *Chem.–Eur. J.*, 2013, **19**, 14416.

46 M. Ousmane, G. Perrussel, Z. Yan, J. M. Clacens, F. De Campo and M. P. Titus, *J. Catal.*, 2014, **309**, 439.

47 A. Tanksale, J. N. Beltramini, J. A. Dumesic and G. Q. Lu, *J. Catal.*, 2008, **258**, 366.

48 S. Abate, K. Barbera, E. Giglio, F. Deorsola, S. Bensaid, S. Perathoner, R. Pirone and G. Centi, *Ind. Eng. Chem. Res.*, 2016, **55**, 8299.

49 S. Velu and S. K. Gangwal, *Solid State Ionics*, 2006, **177**, 803.

50 C. P. Li, A. Proctor and D. M. Hercules, *Appl. Spectrosc.*, 1984, **38**, 880.

51 E. Heracleous, A. F. Lee, K. Wilson and A. A. Lemonidou, *J. Catal.*, 2005, **231**, 159.

52 G. Li, L. Hu, J. M. Hill, G. Li, L. Hu and J. M. Hill, *Appl. Catal., A*, 2006, **301**, 16.

53 S. R. Bare, S. D. Kelly, F. D. Vila, E. Boldingh, E. Karapetrova, J. Kas, G. E. Mickelson, F. S. Modica, N. Yang and J. J. Rehr, *J. Phys. Chem. C*, 2011, **115**, 5740.

54 B. C. Vicente, R. C. Nelson, A. W. Moses, S. Chattopadhyay and S. L. Scott, *J. Phys. Chem. C*, 2011, **115**, 9012.

55 A. Fouskas, M. Kollia, A. Kambolis, C. Papadopoulou and H. Matralis, *Appl. Catal., A*, 2014, **474**, 125.

56 M. Wu and D. M. Hercules, *J. Phys. Chem.*, 1979, **83**, 2003.

57 J. L. Ewbank, L. Kovarik, F. Z. Diallo and C. Sievers, *Appl. Catal., A*, 2015, **494**, 57.

58 K. Chayakul, T. Srithanratana and S. Hengrasmee, *Catal. Today*, 2011, **175**, 420.

59 G. Garbarino, C. Wang, I. Valsamakis, S. Chitsazan, P. Riani, E. Finocchio, M. F. Stephanopoulos and G. Busca, *Appl. Catal., B*, 2015, **174**, 21.

60 J. Okal, L. K. Piński, L. Krajczyk and W. Tylus, *J. Catal.*, 2003, **219**, 362.

61 J. Okal, W. Tylus and L. Kępiński, *J. Catal.*, 2004, **225**, 498.

62 G. Beamson, A. J. Papworth, C. Philipps, A. M. Smith and R. Whyman, *J. Catal.*, 2011, **278**, 228.

63 P. Salagre, J. L. G. Fierro, F. Medina and J. E. Sueiras, *J. Mol. Catal. A: Chem.*, 1996, **106**, 125.

64 J. Zieliński, *J. Catal.*, 1982, **76**, 157.

65 D. Chang and F. A. Sherrod, *US Pat.*, 5 817 593, The Dow Chemical Company, 1998.

66 A. M. Hilmen, D. Schanke and A. Holmen, *Catal. Lett.*, 1996, **38**, 143.

67 F. F. Yang, D. Liu, H. Wang, X. Liu, J. Y. Han, Q. F. Ge and X. L. Zhu, *J. Catal.*, 2017, **349**, 84.

68 D. Hibbitts, Q. Tan and M. Neurock, *J. Catal.*, 2014, **315**, 48.

69 J. Lif, M. Skoglundh and L. Löwendahl, *Appl. Catal., A*, 2002, **228**, 145.

70 K. Liu, J. Pritchard, L. Lu, R. van Putten, M. W. G. M. Verhoeven, M. Schmitkamp, X. Huang, L. Lefort, C. J. Kiely, E. J. M. Hensen and E. A. Pidko, *Chem. Commun.*, 2017, **53**, 9761.

71 F. B. Gebretsadik, J. Llorca, Y. Cesteros and P. Salagre, *ChemCatChem*, 2017, **9**, 1.